Hindawi
International Journal of Polymer Science
Volume 2018, Article ID 2385725, 13 pages
https://doi.org/10.1155/2018/2385725

Research Article

Experimental and Numerical Study on the Compression Behavior of Square Concrete-Filled Steel Tube Stub Columns with Steel Fiber-Reinforced High-Strength Concrete

Hyung-Suk Jung,[1] **Baek-Il Bae**,[2] **Hyun-Ki Choi**,[3] **Joo-Hong Chung**,[4] **Chang-Sik Choi**,[5] **and Yun-Cheul Choi**[6]

[1]*Department of Architectural Engineering, Catholic Kwandong University, Gangneung, Gangwon-do, Republic of Korea*
[2]*Research Institute of Industrial Science, Hanyang University, Seoul, Republic of Korea*
[3]*Department Fire and Disaster Prevention Engineering, Kyungnam University, Changwon, Gyeongsangnam-do, Republic of Korea*
[4]*Department of Architecture, Sahmyook University, Seoul, Republic of Korea*
[5]*Department of Architectural Engineering, Hanyang University, Seoul, Republic of Korea*
[6]*Department of Architectural Engineering, Chungwoon University, Incheon, Republic of Korea*

Correspondence should be addressed to Yun-Cheul Choi; 21ycchoi@chungwoon.ac.kr

Received 3 March 2018; Accepted 22 April 2018; Published 11 June 2018

Academic Editor: Aamer Bhutta

This study was conducted to evaluate the applicability of concrete-filled steel tube (CFT) columns made from high-performance construction materials. KBC2016, South Korea's current building code, limits the maximum compressive strength of concrete at 70 MPa and the maximum yield strength of steel at 650 MPa. Similar restrictions to material properties are imposed on major composite structural design parameters in other countries worldwide. With the recent acceleration of the pace of development in the field of material technology, the compressive strength of commercial concrete has been greatly improved and the problem of low tensile strength, known to be the major limitation of concrete, is being successfully addressed by adding fiber reinforcement to concrete. Therefore, the focus of this study was to experimentally determine the strength and ductility enhancement effects, which depend on material composition. To this end, we performed concentric axial loading tests on CFT stub columns made from steel with a yield strength of 800 MPa and steel fiber-reinforced high-strength concrete. By measuring the strain at the yield point of CFT steel during the test, we could determine whether steel yields earlier than ultimate failure load of the member, which is a key design concept of composite structures. The analysis results revealed that the yield point of steel preceded that of concrete on the stress-strain curve by the concurrent action of the strain increase at the maximum strength, attributable to the high compressive strength and steel fiber reinforcement, and the strain increase induced by the confining stress of the steel tube. Additionally, we performed parametric study using ABAQUS to establish the broad applications of CFT using high-performance materials, with the width-to-thickness ratio as the main parameter. Parametric study was undertaken as experimental investigation was not feasible, and we reviewed the criteria for limiting the width-to-thickness ratio as specified in the current building code.

1. Introduction

In line with the continuous trend toward high-rise buildings and long-span structures, it is becoming increasingly necessary to develop high-strength and high-performance materials. Development of high-performance construction materials is an essential factor enabling the construction industry to build ultrahigh buildings and ultra-long-span structures and can contribute to fundamentally solving the issue of securing usable floor space, caused by increased member sizes. In particular, for ultrahigh buildings requiring vertical members with large cross-sections, high-performance materials can allow this cross-section to be reduced. This is reflected in the recent trend of column cross-section design for large-scale structures based on the use of high-performance materials and increasing

demand for composite cross-sections designed to maximize material performance.

However, current design codes [1–4] prescribe the upper and lower limits of material strength in the design of composite members, as well as systems combining structural steel and streel-reinforced concrete. This can be ascribed to the conservatism of design codes, which basically apply conservative requirements and criteria on the basis of various research reports when evaluating untested design elements [5–10]. The reason for such restrictions on material strengths is the change in strain at the maximum strength when the compressive strength of concrete exceeds 70 MPa in the ultimate strength calculation, according to existing research results. Furthermore, a maximum allowable yield strength is applied to members subjected to compressive loads to reflect the difficulty of inducing the yield of steel before that of concrete at a design yield strength exceeding 650 MPa. In cases where the material strength levels deviate from those of the test results from previous studies as reviewed by the building code, it is recommended to ensure security through separate testing or to reduce the design yield strength and compressive strength to the imposed limits. To err on the side of safety, it is general practice to opt for the latter method; however, this approach is tantamount to losing the advantages gained by using high-performance materials as described above. In order to leverage the advantages of high-performance materials, it is therefore of paramount importance to perform experiments to test the actual effects of high-performance materials when their strengths exceed the maximum strength allowed by the building code. This is especially important for high-strength steel, given the necessity to use it along with high-strength concrete (HSC) to enhance the performance of the compressive strength of concrete.

The major problem associated with the use of high-strength steel for rectangular CFT is the strain capacity of concrete. In general, the strain capacity of concrete in CFT is greatly enhanced owing to the enlarged confinement zone in concrete compared with steel-reinforced concrete. According to EC2 [11], however, as the compressive strength of concrete increases, the local strain in specific sections decreases during maximum strength development, which may make it difficult to apply CFT to HSC.

There has been continuous research into steel-reinforced concrete since its development in the 1960s [12], and it is now a common construction material. The ultimate failure of concrete subjected to uniaxial compression is caused not only by compressive stress but also by cracks triggered by lateral expansion under compressive loads. In this process, steel fiber-reinforced concrete contributes to increasing the initial strength of crack generation by tensile force, whereas HSC contributes to preventing spalling through high density owing to the crosslinking effect of steel fiber [13–16].

With this background, this study was conducted to investigate the applicability of HSC for high-strength steel rectangular CFT. The study aimed to evaluate the possible contribution of steel fiber reinforcement to solving the problem of insufficient strain capacity of concrete that may result from the use of HSC. To this end, we performed experiments on rectangular CFT stub columns made from high-performance materials. Additionally, finite element analysis was performed to investigate the effect of CFT using high-performance materials depending on the width-to-thickness ratio, which is one of the important factors by which the yield strength is influenced in the design standards.

2. Limitation of Material Strength and Axial Strength according to Code Provisions

According to South Korea's current building code (KBC 2016) [1], the compressive strength of CFT columns can be calculated from the flexural buckling limit state depending on the slenderness ratio. Specification for Structural Steel Buildings of the American National Standards Institute (ANSI/AISC 360-16) [3] also sets forth an approach to calculating the strength of members taking account of the slenderness ratio. Specifically, when the ratio of the strength of section to the elastic critical buckling load, which represents the slenderness ratio of the member, is less than or equal to 2.25, (2) is used to calculate the compressive strength, and if it exceeds 2.25, (3) is to be used. This is identical to the calculation method presented in KBC 2016. For noncompact sections, the compressive strength of composite columns is to be calculated in two categories of local buckling and its absence. For slender members, since the slenderness of steel is determined by the width-to-thickness ratio, the compressive strength of the section is to be calculated according to the slenderness ratio of each component part.

The strength of compact sections, whose width-to-thickness ratio is smaller than $2.26\sqrt{E/F_y}$, is to be calculated using

$$P_{n0} = P_p = A_s F_y + A_{sr} F_{yr} + 0.85 A_c f_{ck}, \tag{1}$$

where P_{n0} is the nominal axial compressive strength of the section (N), P_p is the superimposed strength of the section (N), F_y is the yield strength of steel (MPa), A_s is the area of steel cross section (mm2), f_{ck} is the compressive strength of concrete (MPa), A_c is the area of concrete cross section (mm2), A_{sr} is the area of continuous rebar (mm2), and F_{yr} is the yield strength of the rebar (MPa).

The strength of the noncompact section, whose width-to-thickness ratio falls within the range of $3.00\sqrt{E/F_y}$ and $5.00\sqrt{E/F_y}$, is to be calculated using

$$P_{n0} = P_p - \frac{P_p - P_y}{(\lambda_r - \lambda_p)} (\lambda - \lambda_p)^2, \tag{2}$$

where λ is the slenderness ratio of the element, λ_p is the limiting width-to-thickness parameter for compact element ($2.26\sqrt{E/F_y}$), λ_r is the limiting width-to-thickness parameter for noncompact element ($3.00\sqrt{E/F_y}$). P_y denotes the axial yield strength of the column (N) and is to be calculated using

$$P_y = F_y A_s + 0.7 f'_c \left(A_c + A_{sr} \frac{E_s}{E_c} \right), \quad (3)$$

where E_s and E_c denote the moduli of elasticity (MPa) of steel and concrete, respectively.

The nominal strength of the slender section, whose width-to-thickness ratio exceeds $3.00\sqrt{E/F_y}$ (lower limit) and smaller than or equal to $5.00\sqrt{E/F_y}$ (upper limit), is to be calculated using

$$P_{n0} = F_{cr} A_s + 0.7 f'_c \left(\frac{E_s}{E_c} \right), \quad (4)$$

where F_{cr} is the critical stress, which is determined as follows in case of a rectangular cross-section:

$$F_{cr} = \frac{9E_s}{(b/t)^2}, \quad (5)$$

where b is the width of element exposed to compression (mm) and t is the thickness of plate (mm).

A strength reduction factor of 0.75 is to be applied and the percentage of steel in the total cross-sectional area must exceed 1%.

It was found that the same limits are applied to concrete compressive strength in KBC2016 [1] and ANSI/AISC 360-16 [3]: the lower and upper limits are 21 MPa and 70 MPa, respectively, for normal-weight concrete, and the upper limit for lightweight concrete is 42 MPa. As for the yield strength of steel, however, the two codes set forth different upper limits: KBC2016 [1] prescribes the design yield strength of structural steel used for calculating the strength of composite columns not to exceed 650 MPa and ANSI/AISC 360-16 [3] limits the maximum yield strength of structural steel and steel reinforcement to 525 MPa and 550 MPa, respectively.

3. Compression Test of Rectangular CFT Stub Columns Using High-Performance Materials

3.1. Experiment Design. To determine the applicability of rectangular CFT made from high-performance materials in view of the provisions of the design codes as reviewed above, compression testing was performed on rectangular CFT columns made from high-performance materials. A total of eight experiments were performed, with the compressive strength of concrete, type of steel, and content level of steel fiber as independent variables. The specifications of the specimens are shown in Figure 1, and those of each variable are outlined in Table 1.

Two types of steel that differed in yield strength, SM490 and HSB800, were used to evaluate the effect of enhanced yield strength on the compressive strength development. The design compressive strength of HSC was set at 100 MPa, and ultra-high-strength concrete (UHSC) implementing the concept of reactive powder concrete (RPC) was fabricated in an attempt to induce a compressive strength development exceeding 100 MPa [17]. Table 2 presents the concrete blending ratios for fabricating the test specimens. As steel fiber reinforcement, we used straight

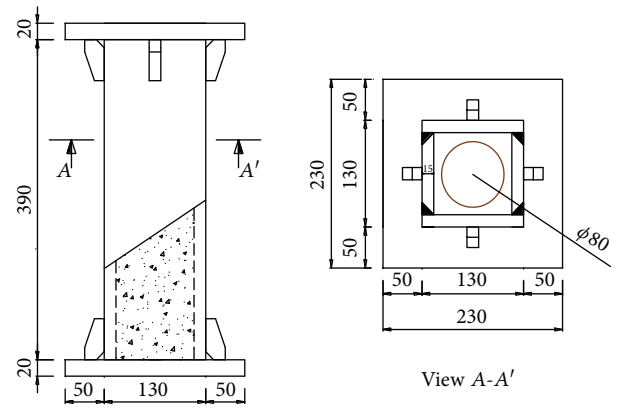

Figure 1: Details of test specimens.

Table 1: Variables and details of test specimens.

Specimen	b/t	f'_c(MPa)	F_y (MPa)	Partial concrete strength (χ)	P_{cal}
HS-800	6.7	0	879	NA	5472
CS-800-3	6.7	30	879	0.05	5725
CS-800-10	6.7	102	879	0.14	6328
CS-800-F10	6.7	102	879	0.14	6328
HS-490	6.7	0	360	NA	2165
CS-490-3	6.7	30	360	0.11	2418
CS-490-10	6.7	102	360	0.29	3024
CS-490-F10	6.7	102	360	0.29	3024

b: width of column section; t: thickness of steel; f'_c: compressive strength of concrete; F_y: yield strength of steel; $\chi = (A_c f'_c)/(A_s F_y)$; A_c: sectional area of concrete; A_s: sectional area of steel; P_{cal}: calculated strength of test specimen based on KBC2016.

brass-coated fibers (13 mm length and 0.2 mm diameter) with a tensile strength of 2600 MPa, mixing them at a 2% volume ratio normally applied to UHSC. A hollow rectangular steel tube specimen was additionally fabricated for each steel type in order to determine the effect of concrete filling on strength enhancement. We applied additional reinforcement to the end parts of the specimens to prevent early failure at both ends during buckling. For the HSB800 steel, specially designed welding rods were used.

3.2. Material Test. The main objective of this study was to evaluate the applicability of high-performance materials. Therefore, it is important to define the properties of the high-performance materials used. To this end, we performed tests on each of the steel and concrete materials to be used for the compression test. The experiments on the mechanical properties of steel were carried out in compliance with KS B 0801 and 0802 [18, 19]. Specifically, in order to investigate the increase in compressive strength and tensile strength induced by mixing steel fibers into HSC, we measured experimentally the compressive strength, splitting tensile strength, and flexural tensile strength among the mechanical properties of concrete, in compliance with the test methods stipulated in KS F 2405 [20], KS F 2423 [21], and JCI-S-001 [22], respectively.

Table 2: Mix proportions of concrete.

ID	W/B (HSC) W/C (NSC) (%)	C	W	SF	S	F	G	SP	StlF
					Unit weight (kg/m^3)				
3	0.25	809	222	80	1052	162		3.01	
10/F10	63.2	348	220		1065		666	2.85	157 (100F)

W/B: water binder ratio; W/C: water cement ratio; C: cement; W: water; SF: silica fume; S: fine aggregated; F: filler; G: coarse aggregate; SP: super plasticizer; StlF: steel fiber (volume fraction %).

Table 3: Mechanical properties of steel.

Steel	F_y (MPa)	F_u (MPa)	F_y/F_u	Elongation (%)
HSB800	879	944	0.93	22
SM490	360	506	0.70	26

F_y: yield strength of steel; F_u: ultimate strength of steel.

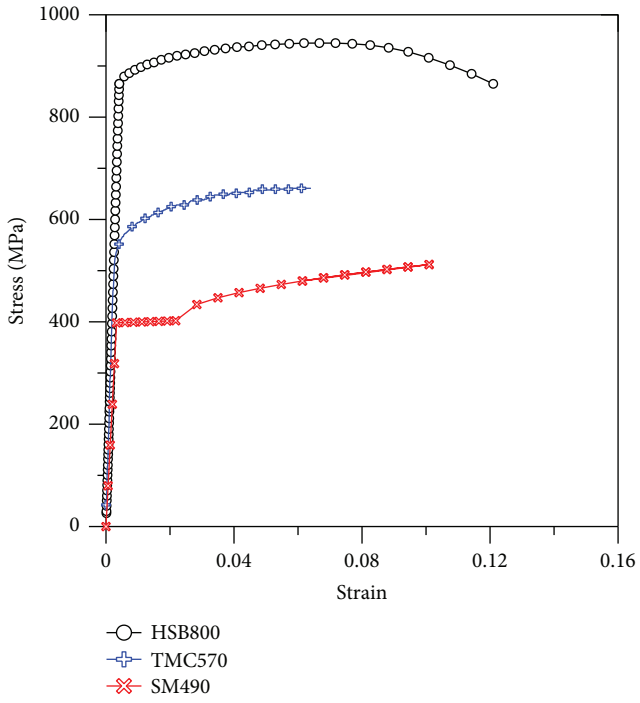

Figure 2: Stress-strain relation of steel.

Table 4: Mechanical properties of concrete.

ID	E_c	f_c' (MPa)	f_{sp}	f_r	Remarks
3	29041	33.02	5.02	7.62	No fiber
10	36233	102.38	7.86	11.54	No fiber
F10	38099	104.87	10.50	16.50	$V_f = 2.0\%$

f_c': compressive strength tested according to KS F 2405; f_{sp}: splitting strength tested according to KS F 2423; f_t: flexural tensile strength tested according to JCI-S-001-2003.

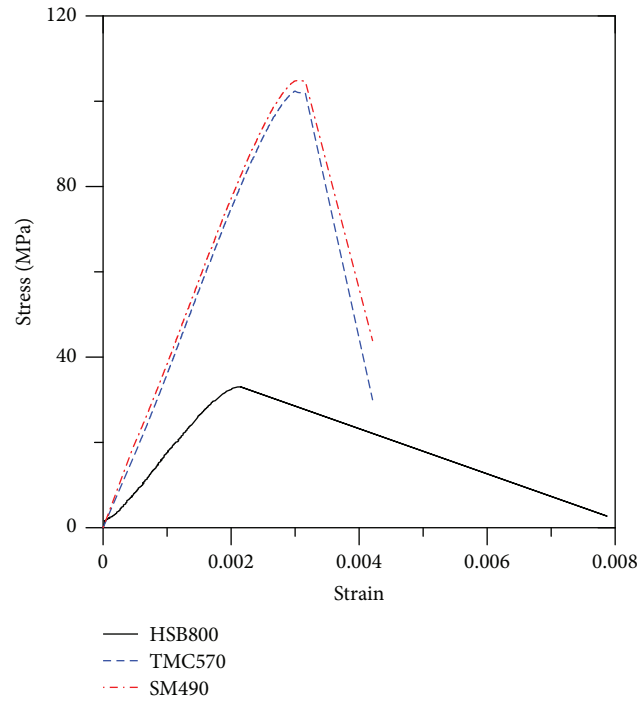

Figure 3: Stress-strain relation of concrete.

The results of the tests on steel types used in the experiments are outlined in Table 3. The stress-strain relationship of the high-strength steel HSB800 was compared with that of SM490 and SM570TMC, and the results are plotted in Figure 2. As shown in Figure 2, steel HSB800 is no-yield-point steel, that is, it does not show any clear yield point as does SM570TMC steel, and has a higher yield ratio than SM490. Consequently, its yield strength was calculated using the 0.2% offset method used for defining the yield strength of typical high-strength steel.

Table 4 outlines the measurement results of the compressive strength, splitting tensile strength, and flexural tensile strength of concrete. Specifically, the results of compression test are expressed by the stress-strain relationship as plotted in Figure 3. Three matrices were used in total. In the concrete matrix with a compressive strength of 30 MPa, generally classified as ordinary strength concrete, the load supporting capacity was found to decrease slowly without occurrence of any sudden decrease in load supporting capacity after the maximum strength development. In contrast, HSC was observed to lose the entire load supporting capacity due to spalling which occurred concurrently with the maximum strength development. However, no spalling appeared when

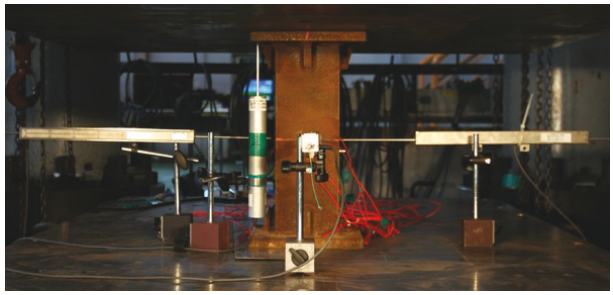

Figure 4: Test setup.

HSC was reinforced by steel fibers; although the load supporting capacity was considerably reduced after the maximum strength was reached, a complete loss did not occur. It was also found that the steel fiber reinforcement contributed to increasing the splitting tensile strength and flexural tensile strength by a factor of 1.33 and 1.42, respectively, when compared with the specimens not reinforced by steel fiber.

3.3. Test Setup and Measurement Plan. For the experiments, we used a universal testing machine (UTM) with a capacity of 10000 kN, taking account the axial strength of the specimens. Experiments were carried out in the form of uniaxial compression testing of each specimen. Figure 4 shows the test setup of the specimens. The load acting on the specimen was obtained with the load cell of the UTM, and the values of the vertical displacement at the top of the specimen and the lateral expansion at the center were obtained using linear variable differential transformer (LVDT) sensors. Strain gauges were installed at the center part to obtain the strain of the steel. The measurement plan is outlined in Figure 5.

4. Test Results and Discussion

Figure 6 illustrates the failure modes of the specimens at each load increment. All specimens (HS-800, HS-490, CS-800 series, and CS-490 series) went through the same pattern of failure modes. The load increased from the initial elastic slope up to the postyielding strain hardening zone and then decreased with the onset of local buckling. Ultimately, the load on the specimen decreased sharply with the onset of weld fracture. In all four specimens, no weld fracture was observed until the ultimate strength was reached. Figure 6 shows the specimens after the completion of the experiments [23].

The composite section of the HSB800 CFT stub column tested does not undergo fracture unlike brittle materials due to the effect of its perfectly plastic stress-strain behavior $(b/t = 6.7 < \lambda_{p,HSB800} = 17)$. Accordingly, the yield strength was determined by the 1/3 stiffness method, tangential method, and 0.2% offset method for the efficient analysis of the test results. The three yield strength determination methods are presented in Figure 7. Of them, the 1/3 stiffness method was regarded as being most appropriate from the safety point of view and was used for calculating the yield strength of the members and the analysis of the experimental results. Table 5 outlines the yield strengths of the specimens obtained using these three methods.

4.1. Load-Displacement Relation. The load-displacement relations are plotted in Figure 8. The load-displacement curves were used for calculating the maximum strength. All three specimens with composite sections (CS-800-3, CS-800-10, and CS-800-F10) showed an approximately 10% increase in strength when compared with the hollow steel tube specimen (HS-800). However, they showed no significant intergroup differences in the load-displacement relations. This is assumed to be the result of the small ratio of contribution of the steel-governed composite section to strength due to the width-to-thickness ratio and material strength. However, with regard to the material strength composition, it was found that the high-strength steel section did not show any significant differences in strength at a width-to-thickness ratio of 6.7 regardless of whether filled with low-strength concrete (LSC) or HSC. In other words, in the case of high-strength steel CFT, it is not necessary to fill the tube with HSC because it demonstrates the same strength enhancement effect when filled with LSC. This finding is based on a small width-to-thickness ratio and is not enough for drawing general conclusions.

CS-490 series specimens showed different patterns of load-displacement relations depending on the concrete strength. The CS-490-F10 specimen exhibited superior values compared with other specimens in both strength and strain, demonstrating that the strength of the steel fibers mixed into concrete contributes to enhancing its strength and strain. These results lead to the assumption that the ratio of contribution of concrete to the strength is higher than that of CS-800 series specimens in such a way that concrete contributed to the strength enhancement. Table 5 outlines the initial stiffness, yield strength, and ultimate strength of each specimen and their respective displacements.

4.2. Effect of High-Strength Concrete. As a result of comparing the yield strength and ultimate strength increase rates among all specimens depending on the concrete type, as presented in Table 5 and based on the load-displacement relations, the combination of HSB800 and HSC showed a higher increase rate in the yield strength in comparison with the combination of HSB800 and LSC. The same result was obtained when SM490 was used. In the ultimate strength, however, a higher strength increase rate was demonstrated by the combination of HSB800 and LSC compared with the combination of HSB800 and HSC. This is assumed to be ascribable to the decrease in the effect of confinement with the increase in concrete compressive strength, as demonstrated by earlier studies on the confinement effect of HSC [23–26]. In both steel types, HSC800 and SM490, the increase rate of strain capacity from the onset of yield of the member to the ultimate state was found to be similar regardless of whether the steel was combined with LSC or HSC.

4.3. Effect of Steel Fiber. In an attempt to solve the problems of HSC-inherent brittle fracture behavior and strain

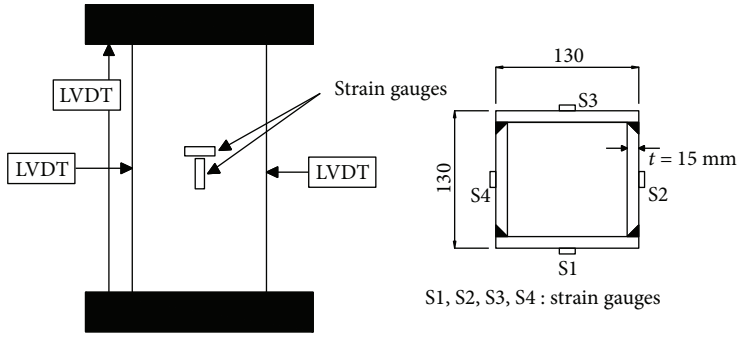

Figure 5: Measurement plan.

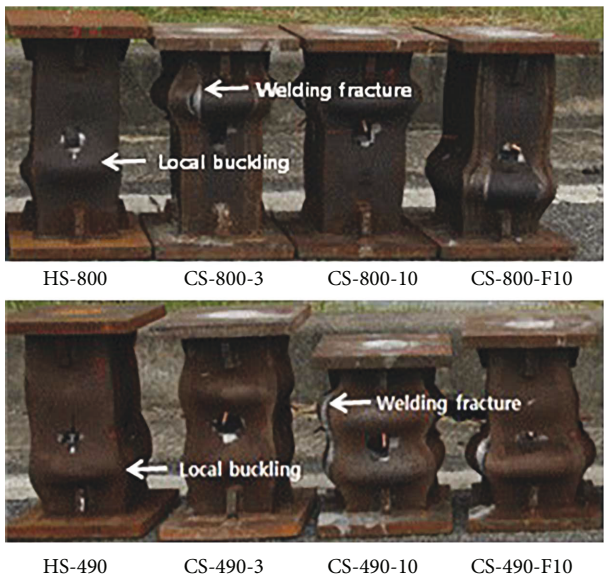

Figure 6: Failure of test specimens.

decrease at the maximum strength, we performed experiments on steel fiber-reinforced specimens. As shown in Figure 3, the strain was found to increase at the maximum strength. HSC specimens did not show any significant strength enhancement in both steel types despite the steel fiber reinforcement. In the case of the ultimate strength, however, SM490 exhibited a higher increase rate after the steel fiber reinforcement. On the other hand, the displacement ratio of the ultimate strength to the yield strength was found to increase after steel fiber reinforcement.

4.4. Change of Failure Pattern. The steel tube used for the specimen fabrication was a 15 mm-thick panel with a small cross-sectional area (130 mm); that is, the composite section of the CFT stub column tends to show steel-governed behavior. Drawing on this, on the assumption that the steel tube part hardly undergoes any change in strength regardless of whether it is filled with concrete or not on the composite section of steel tube and concrete, the value obtained by subtracting the pure strength of the steel tube from the strength of the composite section was defined as the strength under concrete confinement.

As explained in the introduction, the reason for limiting the material strength in the current building code is to enable a design that induces the exterior steel tube to yield earlier than the compression fracture of core concrete. If high-strength steel is used, concrete failure can occur first depending on the strain rate. This is not desirable from a safety point of view and is therefore a point that must be checked when designing HSB800 steel composite members. Given the nature of concrete that increased strength and confinement bring about increase in maximum strain, the strain of the core concrete under confinement explained in the preceding section was indirectly measured and compared with the steel tube strain in order to examine the yield pattern, that is, whether the steel tube yields first. As shown in Figure 9, the maximum strain of the core concrete was found to grow larger than that of the HSC-filled steel tube. This result deviates from the EC2 model, in which the maximum strain decreases as the concrete compressive strength increases, and may be explained by the comparatively low modulus of elasticity of the HSC used in this study, which was fabricated according to the RPC concept. This confirmed the possibility of maintaining the pattern of earlier steel yield complying with the conventional design concept of filling the steel tube with RPC-based 100 MPa concrete. Additionally, as could be confirmed from steel fiber-reinforced material tests, the strain exhibited a higher value at the maximum strength. This is another factor conducive to inducing the earlier yield of steel. From these findings, it may be concluded that rectangular CFTs made from high-strength steel may find safe applications in construction sites when combined with high-strength fiber-reinforced concrete.

5. Finite Element Analysis of Test Specimens and Parametric Study

As mentioned above in Section 4, the CFT-related effect of concrete could not be clearly demonstrated due to the material properties and the limitations of the test equipment [23]. Therefore, we performed numerical analysis to investigate the width-/thickness-dependent behavior changes of the CFT made from high-performance materials, using the commercial finite element analysis (FEA) program ABAQUS [27]. The adequacy of the FEA was tested by comparing the numerical and experimental results obtained in this study, followed by parametric analysis.

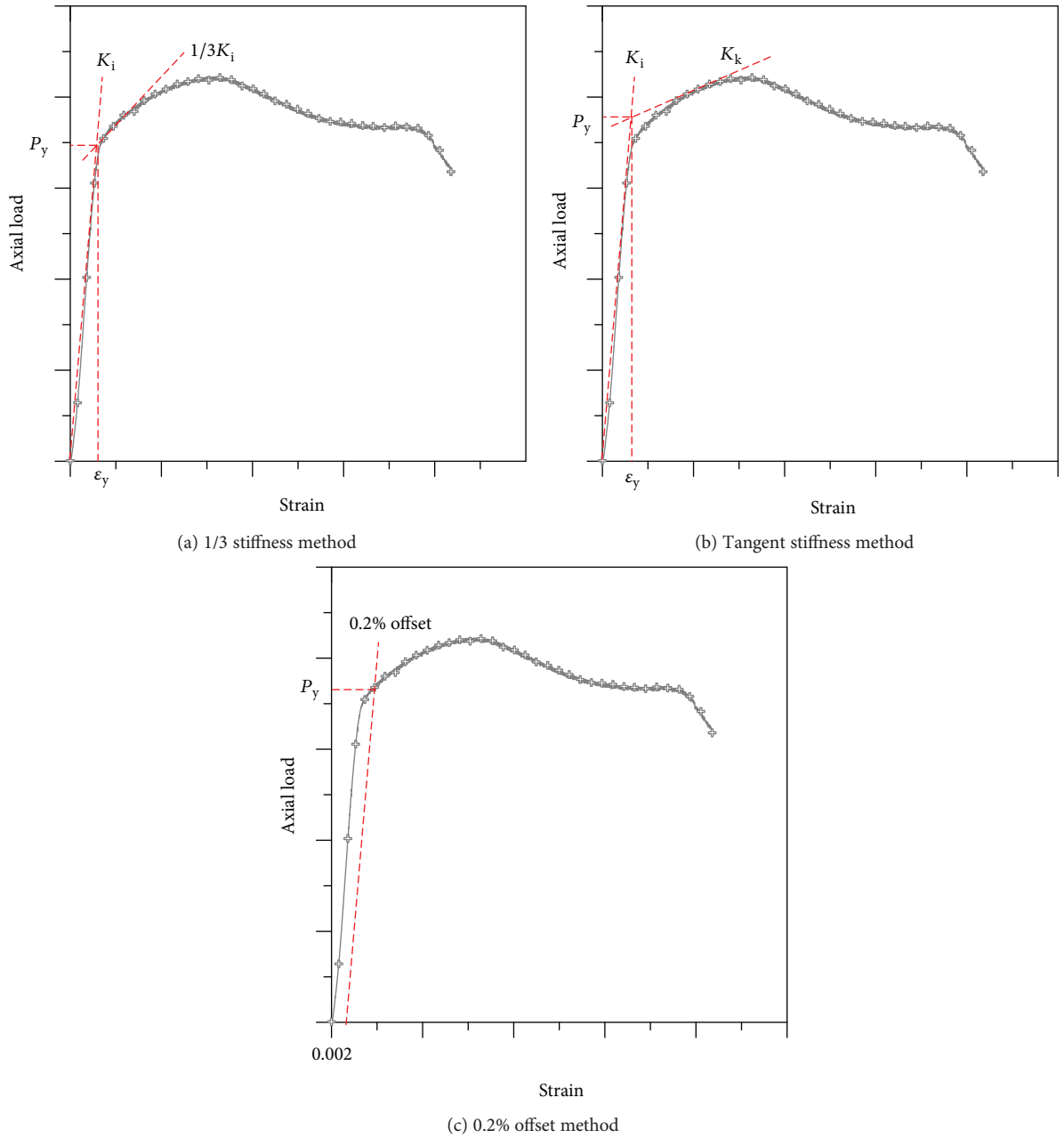

(a) 1/3 stiffness method

(b) Tangent stiffness method

(c) 0.2% offset method

Figure 7: Determination method for yield strength of member.

5.1. Modeling and Verification. Concrete and steel modeling was performed using 3D solid elements. It was judged to be most efficient to model steel with solid elements to directly reflect the changes in the width-to-thickness ratio. As solid elements, we used the eight-node linear brick element C3D8R element provided by ABAQUS [27]. The model was constructed in a manner to express the deformation due to local buckling by using a nonlinear geometry option. As the constitutive law, it was decided to follow the isotropic hardening rule for steel, and for the uniaxial stress-strain relationships, we used the results of experiment performed on each specimen, as presented in Figure 2.

As for the concrete constitutive law, we used the concrete damaged plasticity model [28]. The concrete damaged plasticity model is a model designed to describe the continuum plasticity-based concrete damage; for the purpose of this study, the major failure of concrete was assumed to arise from tensile cracking and compressive fracture. The plastic flow rule, nonassociated, can constitute an asymmetric stiffness matrix and is thus known to express rock-like brittle materials fairly well. Although it cannot express the cracks directly, it was selected for failure modeling because cracks do not play any significant role in this study.

Concrete material behavior can be modeled by inputting the uniaxial loads or the stress-strain relationships in the tensile state. In order to reflect the concrete strength changes, the compressive stress-strain model of Collins and Porasz [29] was used to enable the application of HSC. For modeling

Table 5: Strength of test specimens.

Specimen	P_{cal} (kN)	P_y (kN)	P_u (kN)	d_y (mm)	d_u (mm)	d_u/d_y	k (kN/mm)
HS-800	6007	6038	7632	7.00	28.88	4.13	875
CS-800-3	6261	7025	8402	7.03	31.16	4.43	1062
CS-800-10	6862	7400	8442	8.05	35.76	4.44	1120
CS-800-F10	6862	7627	8553	8.50	38.98	4.59	1125
HS-490	2473	2849	5620	3.79	57.70	15.22	880
CS-490-3	2726	3423	6127	4.50	106.50	23.67	882
CS-490-10	3332	3951	6745	4.68	112.16	23.97	960
CS-490-F10	3332	3958	7322	5.12	139.40	27.23	1040

P_{cal}: calculated test specimen strength based on the code provisions (KBC2016); P_y: yield strength of test specimen; P_u: ultimate strength of test specimen; d_y: axial shortening of test specimen experiencing yield strength; d_u: axial shortening of test specimen experiencing ultimate strength; k: initial stiffness.

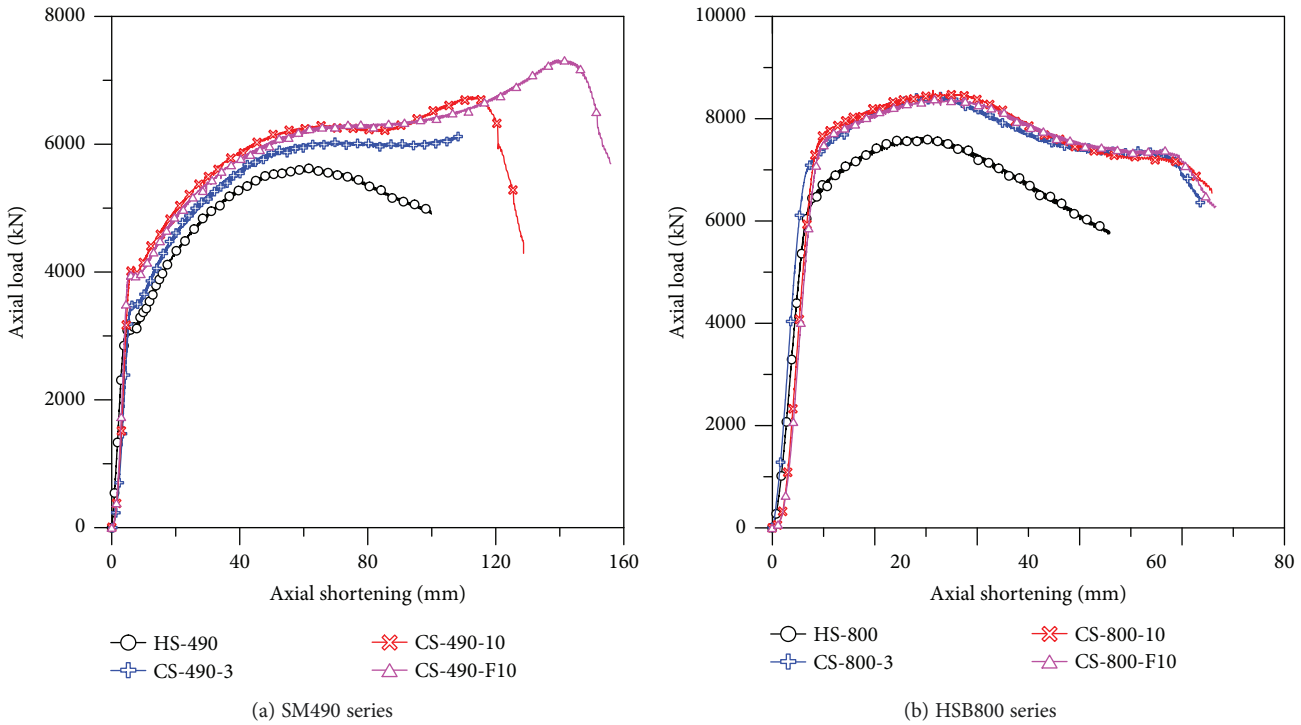

(a) SM490 series (b) HSB800 series

Figure 8: Load-displacement relation.

concrete tensile, the widely used Okamura–Maekawa [30] model was used and the effect of steel fibers was taken from the research results of Lok and Xiao [31]. The modulus of elasticity of concrete was calculated according to the methods provided in the Concrete Design Code (2012) [32], taking account of the link to KBC2016 [1]. The concrete-steel interface was modeled using the contact element. In the tangential direction, the frictional force between concrete and steel was modeled by inputting the friction coefficient of 0.25 proposed by Korea Concrete Institute [33] and modeling in the normal direction, with the mutual nodes of concrete and the steel configured to not permeate. This enabled the modeling of the confinement effect caused by the difference in the Poisson's ratio between steel and concrete. The general displacement control method was used for loading, and the boundary conditions of the both ends of the column analyzed were entered as fixed ends.

Validation of the proposed model is an indispensable part of the process of FEA-based parametric analysis performed for the evaluation of the applicability of high-strength steel. This was done by analyzing the experimental results obtained in this study as well as the experimental results obtained in an earlier study [34] using specimens with compressive strength exceeding 800 MPa. The specimens used in the earlier study were rectangular CFTs (110 × 110 mm) made from HSS2 with a steel yield strength of 750 MPa, concrete compressive strength of 28 MPa, and panel thickness of 5 mm. The length of the specimens was 300 mm. The analysis results of the measured values obtained from the HSS2 specimens in the

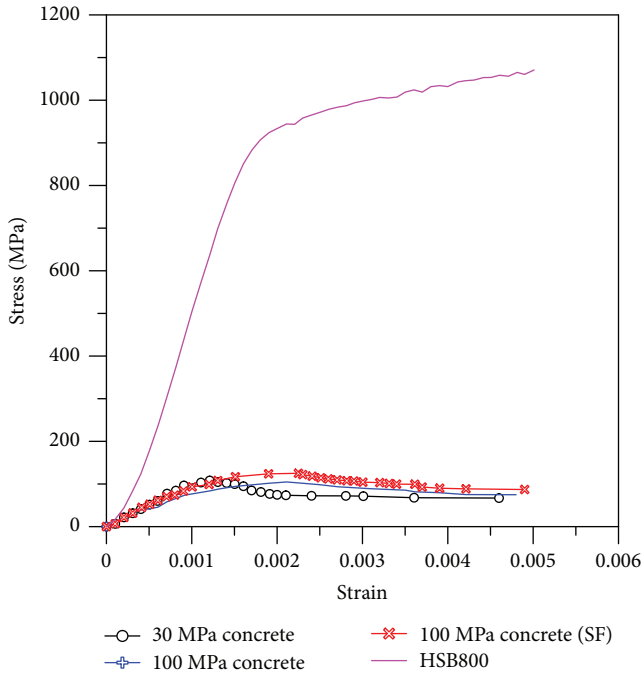

Figure 9: Stress-strain relation of concrete through the test results.

previous study and those obtained in the present study were compared with the numerical analysis results and presented in Figure 10. The comparison of the analysis results between the experimental and numerical values of all tested parameters revealed that the errors in the maximum load modeling were within the range of 10%, thus demonstrating that FEA model can be applied when analyzing the behavior of CFTs made from high-strength materials. The numerical and experimental results obtained from each specimen are outlined in Table 6.

5.2. Failure Pattern with a Different b/t Ratio and Effectiveness of Matrix Strength and Steel Fiber Inclusion. Figure 11 shows the analysis results of two specimens performed in this study, the CSS-800-10 and CSS-800-10, which used high-strength concrete and iron fiber-reinforced high-strength concrete for high-strength steels. Figure 11 showed the stress distribution diagram in the state in which the specimen was about to yield. It is confirmed that if it is not reinforced with steel fibers, as shown in Figure 11(a), the concrete can be converted into a tensile stress without resisting expansion due to compression stress. At the same time, it was found that the compression stress was about to be converted to tensile stress in the steel. On the other hand, it was found that, when mixed with steel fibers, there was no tensile stress on both concrete and steel, but only compressed stress appeared. As can be found in the material test results, this is judged to be the result of increased tensile strength by steel fibers. Accordingly, it is judged that the use of steel fiber may be delayed to buckling by the expansion force due to increased tensile strength of concrete.

The effect of the width-to-thickness ratio of high-strength steel panel on strength and strain was investigated, and the load-displacement relations were normalized for the use of LSC and that of HSC based on the design formulae provided by the current design code; the results of which are plotted in Figures 11(a) and 11(b). It can be confirmed that the maximum strength point varied according to the width/thickness change. As the latter increased, the former occurred earlier. In the case of LSC, in particular, the maximum loads were found to fall short of the calculated values when the width-to-thickness ratio exceeded 50. In the case of HSC, the strength was found to be lower than the design strength when the width-to-thickness ratio exceeded 70. From this, it can be inferred that when high-strength steel is used, the maximum permissible width-to-thickness ratio needs to be reviewed to reflect different levels of concrete compressive strength. Figure 12(c) presents the analysis results for the steel fiber-reinforced HSC obtained to investigate the effect of steel fibers. The steel fiber reinforcement was found to increase not only the maximum load but also the crushing strain of concrete, thus increasing the maximum permissible width-to-thickness ratio when HSC is used. This highlights the need to consider the effect of steel fibers as well when reviewing the maximum permissible width-to-thickness ratio.

6. Conclusion

The main purpose of this study was to evaluate the feasibility of the application of rectangular CFTs made from high-performance materials, as well as their behavior. To this end, we performed experiments on rectangular CFT stub columns using high-strength steel and steel fiber-reinforced ultra-high-strength concrete and performed numerical analysis to investigate the relationship between the width-to-thickness ratio and high-performance concrete, which could not be tested experimentally. From these experimental and numerical processes, the following conclusions could be drawn.

(1) It was confirmed by the experimental results that none of the specimens underwent weld fracture until their ultimate strength was reached and were thus shown to have sufficient strain capacity to resist the ultimate strength of steel, demonstrating that high-strength steel and steel fiber-reinforced high-strength concrete may be used within the test range.

(2) Comparison of the experimentally obtained ultimate loads with the calculated loads led to the finding that experimental values exceeded the values prescribed as per design formulas. Therefore, it is considered reasonable to apply existing design formulas to the composite section of SB800 steel.

(3) Because of the relatively large contribution of steel to strength, concrete filling was not found to bring about any significant degree of strength changes. In the case of using high-strength concrete, only the specimen using SM490 and all specimens using HSB800 showed yield strength enhancement rates

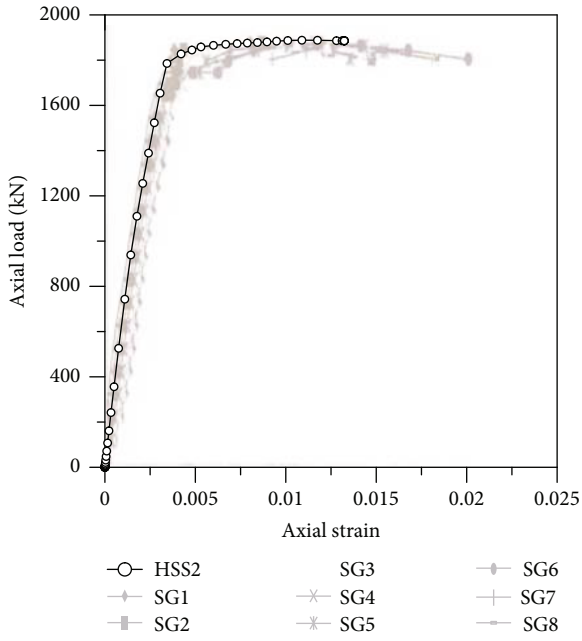

(a) HSS2 specimen

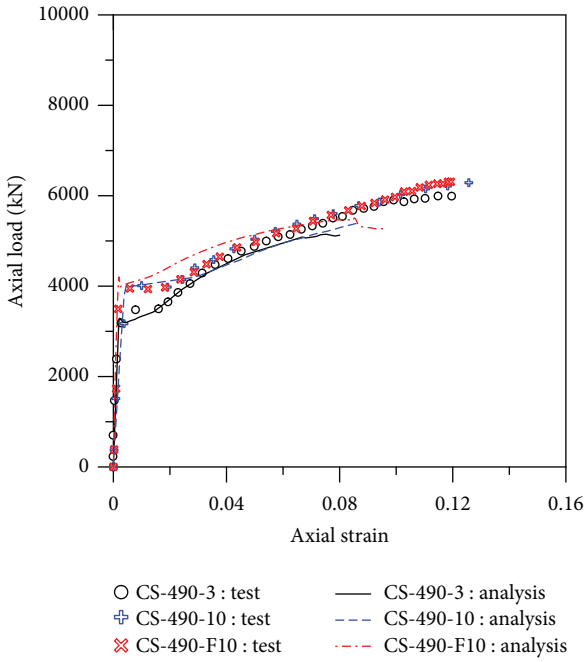

(b) 490 series analysis results

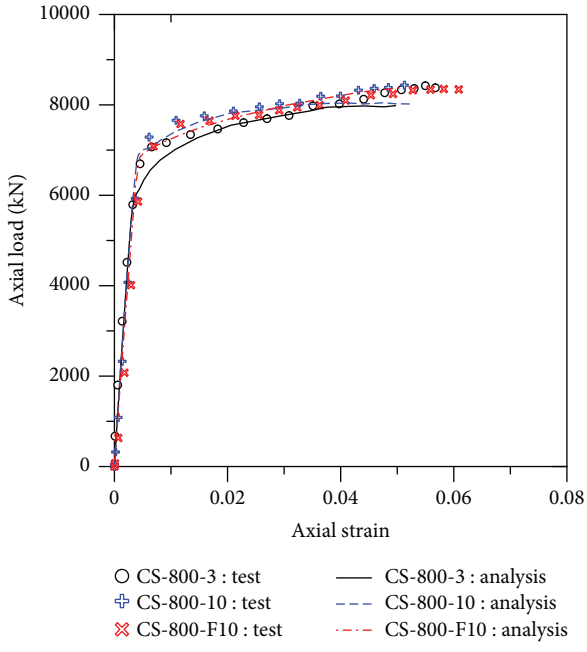

(c) 800 series analysis results

Figure 10: Verification of analysis.

similar to those of normal strength concrete. In strain capacity as well, no significant changes were observed when high-strength concrete was used, presumably because of a low confinement effect in enhancing its strength.

(4) Steel fiber reinforcement was found to have little influence on strength enhancement in all specimens using HSB800 and SM490. This may be ascribable to the negligible strength change in concrete by the steel fiber reinforcement. By contrast, the effect of steel fiber reinforcement was clearly demonstrated in the strain capacity.

(5) Given the nature of concrete that increased strength and confinement bring about increase in maximum strain, the strain of the core concrete under confinement was indirectly measured and compared with the steel tube strain in order to examine the yield pattern, that is, whether the steel tube yields first. As a

Table 6: Comparison between analysis results and test results for CFT specimens.

Specimen	$P_{cal-code}$ (kN)	P_{y-test} (kN)	P_{y-mum} (kN)	P_{u-test} (kN)	P_{u-mum} (kN)
CS-800-3	6261	7025	6560	8402	7984
CS-800-10	6862	7400	7056	8442	8040
CS-800-F10	6862	7627	6943	8553	8386
CS-490-3	2726	3423	3277	6127	5077
CS-490-10	3332	3951	3779	6745	5402
CS-490-F10	3332	3958	3944	7322	5380

$P_{cal-code}$: code-based strength; P_{y-test}: yield strength-test results; P_{y-mum}: yield strength-analysis results; P_{u-test}: ultimate strength-test results; P_{u-mum}: ultimate strength-analysis results.

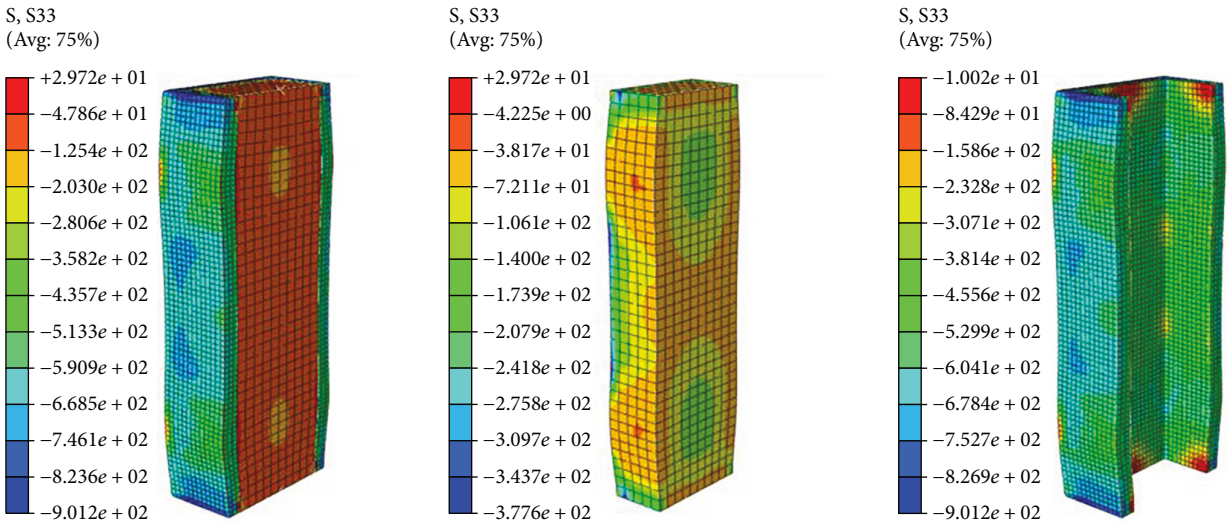

(a) Analysis results of CS-800-10

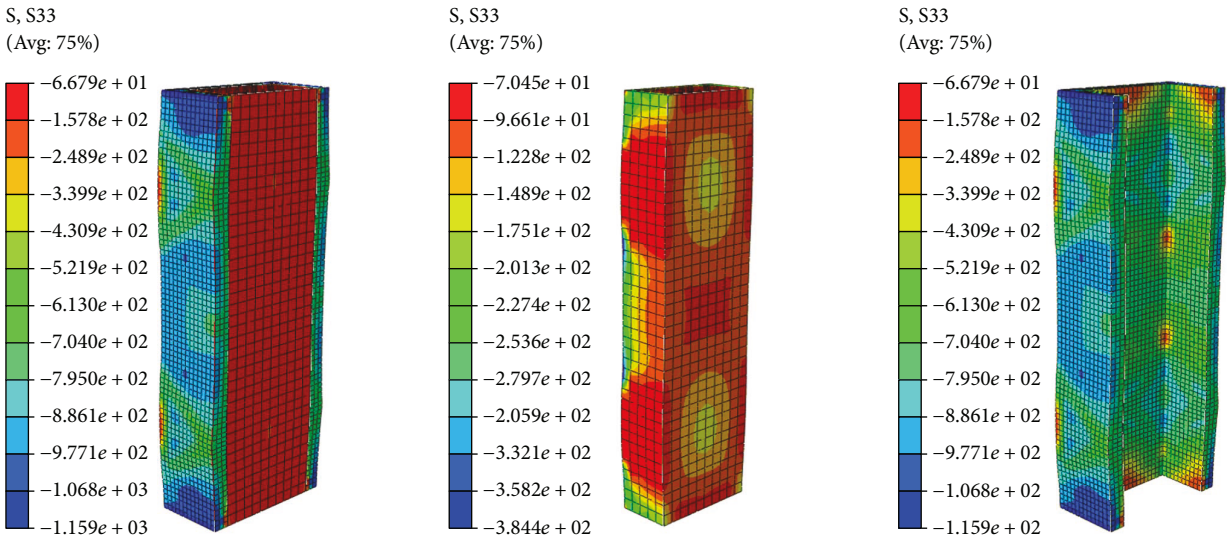

(b) Analysis results of CS-800-F10

Figure 11: Failure aspect of SFRC-filled high-strength steel tube column.

result, it was found that the maximum strain of the core concrete was found to grow larger than that of the steel tube when it was filled with 100 MPa concrete and reinforced with steel fibers.

(6) Finite element analysis was performed to investigate the effect of the width-to-thickness ratio of steel, which could not be investigated experimentally. As a result of this numerical analysis, it was found that

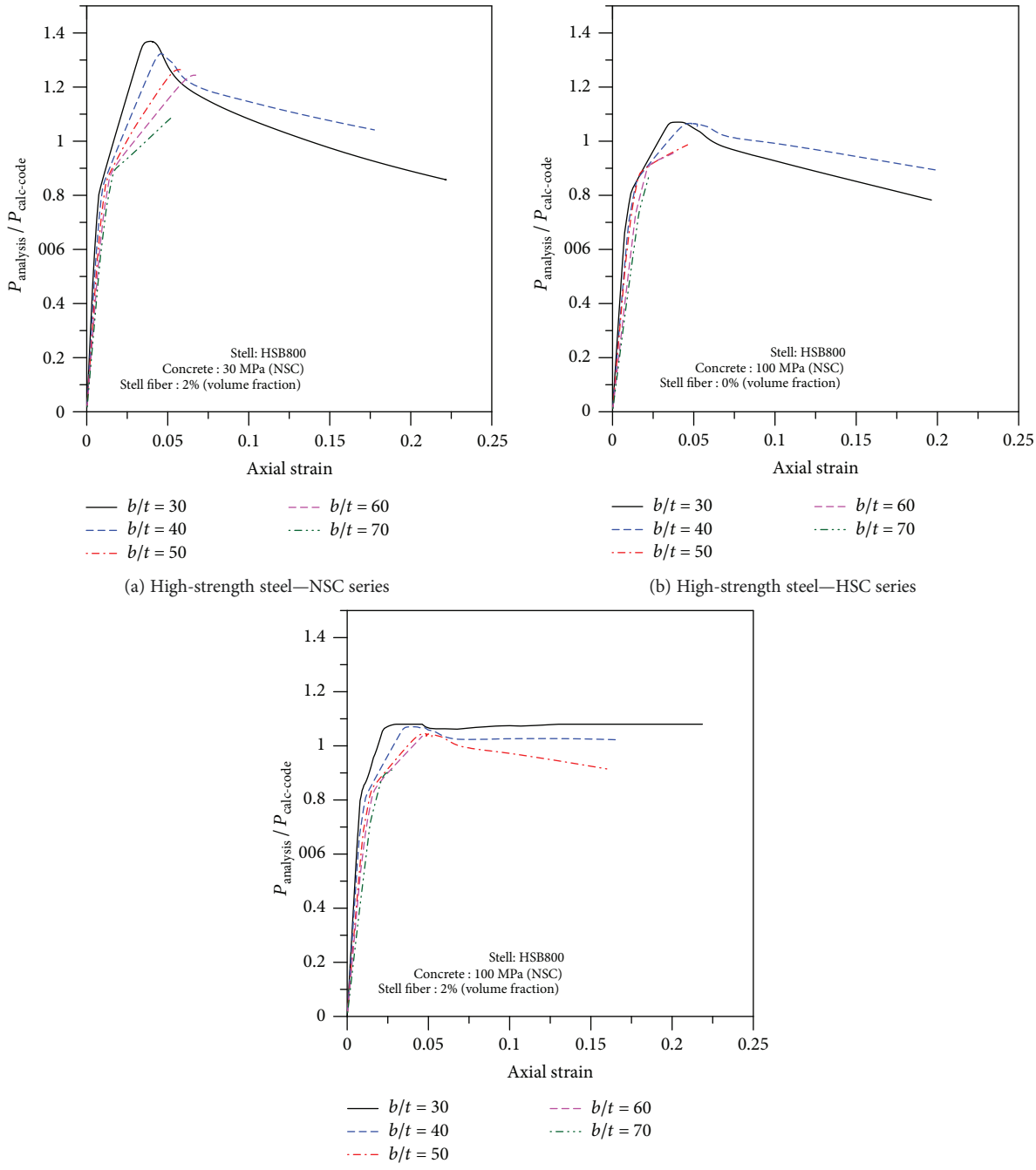

(a) High-strength steel—NSC series

(b) High-strength steel—HSC series

(c) High-strength steel—HSFRC series

Figure 12: Limit b/t ratio according to matrix strength and steel fiber inclusion.

the maximum width-to-thickness ratio permissible for the strength limit set forth by the current building code varied depending on the concrete properties. The maximum permissible width-to-thickness ratio decreased as the concrete strength increased and increased after steel fiber reinforcement.

Conflicts of Interest

The authors declare that they have no conflicts of interest.

Acknowledgments

This work was supported by Chungwoon University Foundation grant, 2017, and the National Research Foundation of Korea (NRF) grant funded by the Korea government (MOE) (NRF-2015R1D1A1A01059989).

References

[1] KBC, *Korean Building Code and Commentary (KBC 2016)*, Architectural Institute of Korea, 2016.

[2] ACI Committee 318, *Building Code Requirements for Structural Concrete (ACI 318-11) and Commentary*, American Concrete Institute, Farmington Hills, MI, USA, 2011.

[3] ANSI/AISC 360-16, *Specification for Structural Steel Buildings*, American Institute of Steel Construction, Chicago, IL, USA, 2010.

[4] European Committee for Standardization, *Eurocode 4: Design of Composite Steel and Concrete Structures*, CEN, 1994.

[5] R. D. Ziemian, Ed., *Guide to Stability Design Criteria for Metal Structures*, John Wiley & Sons, Inc., Hoboken, NJ, USA, 6th edition, 2010.

[6] J. F. Hajjar, "Concrete-filled steel tube columns under earthquake loads," *Progress in Structural Engineering and Materials*, vol. 2, no. 1, pp. 72–81, 2000.

[7] N. E. Shanmugam and B. Lakshmi, "State of the art report on steel–concrete composite columns," *Journal of Constructional Steel Research*, vol. 57, no. 10, pp. 1041–1080, 2001.

[8] A. H. Varma, J. M. Ricles, R. Sause, and L.-W. Lu, "Experimental behavior of high strength square concrete-filled steel tube beam-columns," *Journal of Structural Engineering*, vol. 128, no. 3, pp. 309–318, 2002.

[9] R. T. Leon, D. K. Kim, and J. F. Hajjar, "Limit state response of composite columns and beam-columns part 1: formulation of design provisions for the 2005 AISC specification," *Engineering Journal*, vol. 44, no. 4, pp. 341–358, 2007.

[10] J. R. Kim, S. S. Kim, C. H. Lee, E. T. Lee, and K. Y. Beak, "A study on the material characteristics and the welding properties of 600MPa grade steel (SM 570 TMC)," *Journal of Korean Society of Steel Construction*, vol. 20, no. 6, pp. 773–781, 2008.

[11] European Committee for Standardization, *Eurocode 2: Design of Concrete Structures*, CEN, 1992.

[12] ACI Committee 544, *Measurement of Properties of Fiber Reinforced Concrete*, American Concrete Institute, Farmington Hills, MI, USA, 1988.

[13] B. A. Graybeal, "Compressive behavior of ultra-high-performance fiber-reinforced concrete," *ACI Materials Journal*, vol. 104, no. 2, pp. 146–152, 2007.

[14] P. Bhargava, U. K. Sharma, and S. K. Kaushik, "Compressive stress-strain behavior of small scale steel fibre reinforced high strength concrete cylinders," *Journal of Advanced Concrete Technology*, vol. 4, no. 1, pp. 109–121, 2006.

[15] A. S. Ezeldin and P. N. Balaguru, "Normal- and high-strength fiber-reinforced concrete under compression," *Journal of Materials in Civil Engineering*, vol. 4, no. 4, pp. 415–429, 1992.

[16] B. De Nicolo, L. Pani, and E. Pozzo, "Strain of concrete at peak compressive stress for a wide range of compressive strengths," *Materials and Structures*, vol. 27, no. 4, pp. 206–210, 1994.

[17] P. Richard and M. H. Cheyrezy, "Reactive powder concretes with high ductility and 200 - 800 MPa compressive strength," *Special Publication*, vol. 144, pp. 507–518, 1994.

[18] KS B 0801, *Test Pieces for Tensile Test for Metallic Materials, KS B 0801*, Korean Agency for Technology and Standards (in Korean), 2007.

[19] KS B 0802, *Method of Tensile Test for Metallic Materials, KS B 0802*, Korean Agency for Technology and Standards (in Korean), 2013.

[20] KS F 2405, *Standard Test Method for Compressive Strength of Concrete, KS F 2405*, Korean Agency for Technology and Standards (in Korean), 2010.

[21] KS F 2423, *Method of Test for Splitting Tensile Strength of Concrete, KS F 2423*, Korean Agency for Technology and standards (in Korean), 2006.

[22] JCI-S-001, *Method of Test for Fracture Energy of Concrete by Use of Notched Beam, JCI-S-001*, Japan Concrete Institute Standard, 2003.

[23] C. S. Choi, H. S. Jung, and H. K. Choi, "Behaviour of concrete filled steel square-tube stub column with steel-fiber reinforced high strength concrete," *Advanced Materials Research*, vol. 663, pp. 125–129, 2013.

[24] M. A. Mansur, M. S. Chin, and T. H. Wee, "Stress-strain relationship of high-strength fiber concrete in compression," *Journal of Materials in Civil Engineering*, vol. 11, no. 1, pp. 21–29, 1999.

[25] L. S. Hsu and C. T. Hsu, "Stress-strain behavior of steel-fiber high-strength concrete under compression," *ACI Structural Journal*, vol. 91, no. 4, pp. 448–457, 1994.

[26] G. Campione, S. Mindness, and G. Zingone, "Compressive stress-strain behavior of normal and high-strength carbon fiber concrete reinforced with steel spirals," *ACI Materials Journal*, vol. 96, no. 1, pp. 27–34, 1999.

[27] P. Paultre, R. Eid, Y. Langlois, and Y. Lévesque, "Behavior of steel fiber-reinforced high-strength concrete columns under uniaxial compression," *Journal of Structural Engineering*, vol. 136, no. 10, pp. 1225–1235, 2010.

[28] D. Hibbit, B. Karlsson, and P. Sorensen, *ABAQUS Theory Manual Ver. 6.10.1*, Hibbit, Karlsson and Sorensen, Inc., 2010.

[29] J. Lee and G. L. Fenves, "A plastic-damage concrete model for earthquake analysis of dams," *Earthquake Engineering & Structural Dynamics*, vol. 27, no. 9, pp. 937–956, 1998.

[30] M. P. Collins and A. Porasz, *Shear Design for High Strength Concrete*, The International Federation for Structural Concrete, CEB Bulletin d'Information, No. 193, 1989.

[31] H. Okamura and K. Maekawa, *Nonlinear Analysis and Constitutive Models of Reinforced Concrete*, Gihodo-Shuppan Co., Tokyo, Japan, 1991.

[32] T. S. Lok and J. R. Xiao, "Flexural strength assessment of steel fiber reinforced concrete," *Journal of Materials in Civil Engineering*, vol. 11, no. 3, pp. 188–196, 1999.

[33] Korea Concrete Institute, *Code Requirement and Commentary for Reinforced Concrete Structure*, Korea Concrete Institute, 2012.

[34] E. Ellobody, B. Young, and D. Lam, "Behaviour of normal and high strength concrete-filled compact steel tube circular stub columns," *Journal of Constructional Steel Research*, vol. 62, no. 7, pp. 706–715, 2006.